Modeling the voltage loss mechanisms in lithium-sulfur cells: the importance of electrolyte resistance and precipitation kinetics

Teng Zhang[a,*], Monica Marinescu[a], Laura O'Neill[b], Mark Wild[b], Gregory J. Offer[a]

[a] *Department of Mechanical Engineering, Imperial College London, SW7 2AZ, UK*
[b] *OXIS Energy LTD, E1 Culham Science Centre, Abingdon, OX14 3DB, UK.*

Abstract

Lithium-sulfur (Li-S) cells have the potential to deliver practical energy densities exceeding 400 Wh/kg at cell level in the next few years. However, a lack of understanding of the complex electrochemical, transport, and phase-change phenomena in Li-S cells is arguably holding back development. Acquiring this knowledge requires experimental characterization in tandem with mechanistic modeling. However, existing Li-S models currently contradict some key features of experimental findings, particularly the evolution of cell resistance during discharge. In this study, we demonstrate that, by introducing a concentration-dependent electrolyte conductivity, the correct trends in voltage drop due to electrolyte resistance and activation overpotentials are retrieved. In addition, we reveal the existence of an often overlooked potential drop mechanism in the low voltage-plateau which originates from the limited rate of Li_2S precipitation. Understanding these voltage drop mechanisms is important for correctly interpreting experimental results and for parametrizing advanced mechanistic models. While these effects are exemplified here via a lumped mechanistic model, any existing Li-S models should benefit from including them.

Keywords: Lithium sulfur cells, battery model, precipitation, electrolyte conductivity

1. Introduction

The lithium-sulfur (Li-S) cell could provide the next step-change in battery technology with a promising practical energy density of 500-600 Wh/kg. However, broader uptake of Li-S technology is currently hampered by relatively fast capacity fade, incomplete sulfur utilization, and low Columbic efficiency due to the polysulfide shuttle, among other issues [1, 2, 3, 4, 5]. Improvements in

*Corresponding author
Email address: t.zhang@imperial.ac.uk (Teng Zhang)

battery design and materials research require a good understanding of the complicated electrochemical processes in the Li-S system, which involve multistep reactions, multiscale transport phenomena, and morphology variations during battery operation. Modelling in tandem with experimental testing has been shown to accelerate research and development in the field. [6, 7].

Mikhaylik et al [8] developed the first Li-S model for studying polysulfide shuttle. This lumped model computes reduction potentials in the high and low voltage-plateaus based on the Nernst equation, but it neglects activation overpotentials, electrolyte resistance, and dissolution/precipitation reactions, all which influence the operating voltage. A more detailed one-dimensional (1D) mechanistic model was later described by Kumaresan et al [9] based on the Nernst-Plank equations for dilute solutions. Kumaresan's model considers multicomponent transport in the porous cathode and separator, charge-transfer kinetics, dissolution/precipitation reactions, and changes in porosity and electrochemically active surface area as a result of dissolution/precipitation. While the model qualitatively reproduces some essential features of a typical Li-S discharge profile - such as the two characteristic voltage plateaus and the voltage dip in-between, it also requires the input of a large number of physical and phenomenological parameters that are not easily obtained experimentally. In view of the complexity of the Kumaresan model, Ghaznavi and Chen [10, 11, 12] performed a sensitivity analysis of this model. They concluded that, in order for this model to predict charging, further development in modelling precipitation/dissolution reactions is required. Bessler et al [13, 14] developed a 1D Li-S model based on a similar framework, which additionally considers the electrochemical double-layer, polysulfide shuttle, and irreversible precipitation at the anode as a capacity fading mechanism. In addition to charge/discharge curves, electrochemical impedance spectra at different depths of discharge (DoD) were predicted.

However, while the mechanistic models by Kumaresan et al [9] and Bessler et al [13, 14] can reproduce the general discharge profile of a Li-S cell, they fail to capture more intricate cell behavior such as the changing electrolyte resistance (R_s) during discharge. The variation of R_s with DoD is a characteristic feature of Li-S cells that has been observed in various electrolyte chemistries by electrochemical impedance spectroscopy (EIS) [15, 16, 17, 18]. It is generally agreed that the high-frequency intercept of the EIS curve is dominated by the electrolyte resistance of the measured Li-S cell. As shown in Fig. 1a, during discharge R_s increases in the high plateau and reaches a maximum at the transition between the two voltage plateaus; it then decreases throughout the low-plateau. Furthermore, EIS measurements suggest that R_s accounts for most of the voltage-drop in the high plateau, as the low-frequency resistances – which are frequently associated with charge-transfer - only become significant in the low-plateau [15, 18, 19]. In the mechanistic models, however, the predicted voltage drop due to electrolyte resistance is two to three orders of magnitude smaller than the predicted voltage-drop due to activation overpotentials. Such model prediction, directly contradicting EIS data, is visible in the simulated EIS curves by Bessler et al [13]. The disagreement is also seen for predictions

produced from Kumaresan's model [9], shown in Fig. 1b, where the simulated R_s exhibits a very different evolution with DoD compared to measurements.

The R_s profile during discharge is typically explained with the variation of electrolyte concentration (or viscosity) caused by the dissolution and subsequent precipitation of polysulfide species. Indeed, it was experimentally observed that the electrolyte conductivity of Li-S cells strongly depends on the concentration of both lithium salt [20] and lithium polysulfides [21]. At high salt or polysulfide concentrations (typically $>$ 1 mol/L), increased ionic interactions reduce the electrolyte conductivity. Existing Li-S models, however, rely on dilute solution theory in which ionic conductivities are independent of ionic concentrations.

We propose that introducing a concentration dependence of the electrolyte conductivity is necessary to retrieve the experimentally documented trends in the voltage-drop in Li-S cells during discharge. This feature is included in a lumped mechanistic model that describes electrochemical and precipitation reactions, electrode charge-transfer kinetics, as well as morphology variations due to precipitation in a Li-S cell. Compared to the more detailed Kumaresan model, the lumped model does not consider mass-transport and charge-localization effects, and therefore it cannot predict transport limitations. We note, however, that the sensitivity analysis by Ghaznavi and Chen [12] indicates that mass transport does not have a significant impact on predictions of the Kumaresan model unless ionic diffusion coefficients are reduced by more than an order of magnitude. Consequently, the discharge curves produced by the lumped model closely resemble those obtained with the Kumaresan model. The advantage of the lumped approach is that the model requires fewer fitting parameters and reduced computational resources.

2. Model formulation

The model considers six electrochemical reactions and one precipitation reaction during discharge:

$$\mathrm{Li} \rightarrow \mathrm{Li^+} + \mathrm{e^-} \tag{1}$$

$$0.5\mathrm{S_8} + \mathrm{e^-} \rightarrow 0.5\mathrm{S_8^{2-}} \tag{2}$$

$$2\mathrm{S_8^{2-}} + \mathrm{e^-} \rightarrow 3/2\mathrm{S_6^{2-}} \tag{3}$$

$$\mathrm{S_6^{2-}} + \mathrm{e^-} \rightarrow 3/2\mathrm{S_4^{2-}} \tag{4}$$

$$0.5\mathrm{S_4^{2-}} + \mathrm{e^-} \rightarrow \mathrm{S_2^{2-}} \tag{5}$$

$$0.5\mathrm{S_2^{2-}} + \mathrm{e^-} \rightarrow \mathrm{S^{2-}} \tag{6}$$

$$2\mathrm{Li^+} + \mathrm{S^{2-}} \rightarrow \mathrm{Li_2S} \downarrow . \tag{7}$$

The model considers six electrochemical reactions and one precipitation reaction during discharge:

Eq. 1-6 describes the typical reactions in a catholyte-type cell in which sulfur is initially dissolved in the electrolyte prior to discharge. However, the model can be easily modified to include sulfur dissolution as well as additional

precipitation reactions. The cell voltage can be written as the contribution of three terms:

$$V_{cell} = (E_j + \eta_j) - (E_1 + \eta_1) - IR_s, \text{ for } j = 2 \text{ to } 6 \tag{8}$$

where E_j and η_j are the reduction potential and the activation overpotential for a cathodic reaction j respectively, E_1 and η_1 are the anodic reduction potential and overpotential, and IR_s is the potential drop due to electrolyte resistance. We assume that the Li^+ dissolution kinetics are sufficiently fast such that the anode overpotential η_1 is negligible [13]. All three components are dependent on the species concentrations, C_i, which vary with time due to electrochemical reactions:

$$\frac{d(\varepsilon C_i)}{dt} = a_v \sum_{j=2}^{5} \frac{s_{i,j} i_j}{n_j F}. \tag{9}$$

Here, ε is the spatially-averaged cell porosity, i_j is the current density due to electrochemical reaction j, $s_{i,j}$ is the stoichiometric coefficient of species i in reaction j, n_j is the number of electrons transferred in reaction j, F is the Faraday constant, and a_v is the specific surface area for electrochemical reactions. As this is a 0D model, there is no spatial variation of concentration due to mass transport. The concentration variation of the two species participating in the precipitation reaction in Eq. 7 is given by:

$$\frac{d(\varepsilon C_{S^{2-}})}{dt} = a_v \frac{i_6}{F} - r_p, \;\; C_{Li^+} = C_{Li^+,0} + 2\sum_{i=2}^{8} C_{S_i^{2-}} \tag{10}$$

where r_p represents the precipitation rate of Li_2S, $C_{Li^+,0}$ is the initial Li^+ concentration, and the Li^+ concentration derives from the charge conservation. We employ the expression proposed by Kumaresan et al [9] to describe the rate of precipitation:

$$r_p = k_p v_{Li_2S} (C_{Li^+}^2 C_{S^{2-}} - K_{sp}), \qquad \frac{dv_{Li_2S}}{dt} = -\frac{d\varepsilon}{dt} = V_{Li_2S} r_p. \tag{11}$$

Here, v_{Li_2S} is the volume fraction of Li_2S with respect to cell volume, k_p is the precipitation rate constant, K_{sp} is the solubility product, and V_{Li_2S} is the molar volume of Li_2S. According to Eq. 11, precipitation occurs when the concentration product, $C_{Li^+}^2 C_{S^{2-}}$, exceeds the solubility product, K_{sp}. Furthermore, the rate of precipitation is taken to be proportional to the amount of precipitated Li_2S that provides the necessary surfaces for solid-phase nucleation and growth.

The current densities are related to overpotentials through the Butler-Volmer equation. If the anodic and cathodic transfer coefficients are assumed to both equal 0.5, the current-overpotential relation can be written as:

$$i_j = 2 i_j^0 \sinh(\frac{n_j F}{2RT} \eta_j), \tag{12}$$

in which i_j^0 is the exchange current density for reaction j, R is the ideal gas constant and T is the temperature. Furthermore, the volumetric current densities

due to electrochemical reactions are constrained by the applied current I via:

$$a_v \sum_{j=2}^{6} i_j = \frac{I}{Al}, \tag{13}$$

where A is the apparent geometric area of the cell and l is the cell thickness.

The reduction potential for a reaction j is given by the Nernst equation

$$E_j = E_j^0 - \frac{RT}{n_j F} \sum_j s_{i,j} \ln \left(\frac{C_i}{1 \text{ [mol L}^{-1}]} \right), \tag{14}$$

where E_j^0 stands for the standard reduction potential for reaction j at the reference concentration of 1 mol L^{-1}.

The total electrolyte resistance across the cell can be written as

$$R_s = \frac{l}{A\sigma}, \tag{15}$$

where σ is the electrolyte conductivity. During discharge, electrochemical and precipitation reactions significantly alter the polysulfide concentrations, which in turn influence the electrolyte conductivity. While the exact relation between ionic concentration and electrolyte conductivity has not been established for Li-S cells, it is reasonable to assume that upon increasing Li^+ concentration, the ionic conductivity of the electrolyte first increases and then decreases. This effect is observed in the electrolytes in both lithium-ion and Li-S cells [20, 21, 22]. We further assume cells are usually built with the electrolyte salt concentration close to the optimal value for the maximum electrolyte conductivity (private communication with Oxis Energy LTD). With these assumptions, we propose a linear phenomenological function for σ at high Li^+ concentrations:

$$\sigma = \varepsilon^{1.5} \left(\sigma_0 - b \left| C_{\text{Li}^+} - C_{\text{Li}^+,0} \right| \right). \tag{16}$$

In this expression C_{Li^+} is taken to represent the total ionic concentration of the electrolyte as it equals the sum of anion concentrations. In writing Eq. 15 we have assumed that the electrolyte conductivity is only a function of the total anion concentration (represented by C_{Li^+}) instead of the concentrations of each individual ionic species. This limitation is due to the unknown transport properties of the various polysulfide dianions that may exist during cell discharge. Measuring the properties of individual polysulfide species is challenging due to the complex chemical equilibria among polysulfide species [23]. As shown in Fig. 2a, the electrolyte conductivity reaches the maximum value of σ_0 at Li^+ concentration $C_{\text{Li}^+,0}$, then decreases with slope b.

Finally, we employ the phenomenological expression used by Kumaresan et al [9] to describe the change in specific electrochemical surface area with cathode porosity:

$$a_v = a_{v,0} \left(\frac{\varepsilon}{\varepsilon_0} \right)^{\xi}, \tag{17}$$

where ε_0 is the initial porosity and ξ is a fitting parameter.

The model contains algebraic and ordinary differential equations that can be solved numerically. The model parameters and their assumed values are listed in Table 1. Due to the lack of reported data on standard reduction potentials, exchange current densities, and precipitation kinetics, the parameters in the lumped model - as with the parameters in other Li-S models in the literature - are obtained from calibrating the model with measured discharge curves. Compared to the Kumaresan model [9], the lumped model does not contain the numerous parameters associated with ionic transport, but requires two additional parameters to describe the concentration-conductivity relation.

3. Results and discussion

The simulated discharge curves and electrolyte resistances at 0.15C (0.34A) and 0.03C are illustrated in Fig. 2c-d. Similar to the Kumaresan model [9], the lumped mechanistic model is able to qualitatively reproduce the essential features of the discharge profile of Li-S batteries, e.g. a sloping high-plateau voltage, a flat low-plateau voltage, and a voltage dip in-between. However, the lumped model also reproduces the correct trend and magnitude of the electrolyte resistance during discharge due to the introduction of concentration-dependent electrolyte conductivity. The shape of the resistance profile follows closely the evolution of Li^+ concentration during discharge as shown in Fig. 2b. Initially, as an increasing amount of Li^+ dissolves into the solution to form Li_2S_x, the electrolyte conductivity reduces according to the proposed conductivity-concentration relation Eq. 16. In the low plateau, as Li^+ precipitates out of the solution as Li_2S, the electrolyte conductivity increases. The peak of R_s therefore corresponds to the onset of Li_2S precipitation. It follows that the voltage dip between the voltage plateaus is not only due to the super-saturation of S^{2-} as described by Kumaresan et al [9], but also a consequence of electrolyte resistance peaking at the transition between the two voltage plateaus.

According to Fig. 2d, the peak in electrolyte resistance increases with discharge current. At higher currents, the electrochemical production rates of Li^+ and S^{2-} are faster, whereas their chemical precipitation rate remains the same at the onset of Li_2S precipitation. Consequently, the concentrations of Li^+ and S^{2-} are higher, which gives rise to larger electrolyte resistance for a higher discharge current. It is clear from our analysis that the exact shape of the R_s profile is strongly influenced by the precipitation rate of Li_2S. In the present model, however, the precipitation rate follows Kumaresan's phenomenological expressions Eq. 11, which are known to not reproduce re-dissolution of Li_2S upon charging [11, 12]. A more accurate precipitation/dissolution model would require detailed solid phase nucleation and growth mechanisms as well as experimentally determined solubility products and precipitation rates, values currently not well established in Li-S literature.

The simulated activation overpotentials (defined in Eq. 12) for the high-plateau process reaction Eq. 2 and the low-plateau process reaction Eq. 6 are

shown in Fig. 3. It is clear that the smaller high-plateau overpotential η_2 remains relatively constant in the high plateau whereas the larger low-plateau overpotential η_6 increases with increasing DoD. It is found that the increase in low-plateau overpotential is primarily attributed to the reduction in available electrochemical surface area due to Li_2S precipitation, which is also shown in Fig. 3. As the insulating Li_2S gradually covers a larger portion of the conductive cathode surface, larger activation overpotentials are required to drive the increasing electrochemical current densities. We note that the simulated trend in activation overpotentials resembles that of the low-frequency resistances measured by EIS, which also remain small in the high plateau but rise quickly in the low plateau [15, 18, 19]. Since the activation overpotentials qualitatively reflect the resistance due to charge-transfer, the model agrees with the hypothesis that the low-frequency resistances in EIS measurements arise from charge-transfer processes [15, 18, 19].

In addition to the potential drop associated with the electrolyte resistance and activation overpotentials, a potential shift also occurs due to Li_2S precipitation that alters the reduction potentials in the Nernst equation (Eq. 14). In the absence of precipitation, the S^{2-}concentration increases continuously during discharge in the low plateau, which causes the reduction potentials to drop gradually as dictated by the Nernst equation. This scenario is depicted in Fig. 4 for the low-plateau reduction potential E_6 without precipitation, which is similar to the low-plateau reduction potential calculated by Mikhaylik et al [8]. In the presence of precipitation, the electrochemical production rate of S^{2-} reaches a dynamic equilibrium with its removal rate due to precipitation, thereby holding the S^{2-} concentration and the reduction potential E_6 at relatively a constant values. As illustrated in Fig. 4, the precipitation effectively increases the reduction potential in the low-plateau and gives rise to a flat low-plateau potential. Furthermore, since the precipitation rate is finite, the equilibrium concentration of S^{2-} is higher at higher currents and the reduction potential is correspondingly lower. The limited rate of precipitation effectively manifests as a 'precipitation resistance' that leads to a drop in E_6 at higher currents, as demonstrated in Fig. 4. Due to the quasi steady-state conditions of the testing procedure, EIS measurements do not explicitly reflect reduction potential drop. However, the shift in equilibrium potential has been reported experimentally by the galvanostatic intermittent titration technique (GITT), for which a long voltage relaxation ($\sim$ 40 mV over 20 h) was observed in the low plateau after a current pulse had been removed [24]. This slow potential equilibration was attributed to the slow precipitation/dissolution kinetics in Li-S cells. Since the magnitude of the reduction potential shift is sensitive to the precipitation rate, the GITT technique might be useful for estimating the precipitation rate constants and solubility products needed for more detailed Li-S models.

In the graphical abstract, the three voltage-drop mechanisms considered in the model are shown together for the representative low-plateau reaction Eq. 6. We note that all three mechanisms are related to the precipitation of Li_2S: the precipitation affects the electrolyte resistance and reduction potentials through the change in polysulfide concentrations, and influences activation overpoten-

tials via the change in available electrochemical surface area. For practical, high energy-density Li-S cells, the electrolyte resistance is particularly important since these cells generally contain less electrolyte and therefore higher ionic concentrations [25]. It is therefore important for high energy-density Li-S cells to employ solvents with high ionic conductivities as well as a thin separator to minimize the Ohmic voltage loss. The voltage-drop due to activation overpotentials and the apparent 'precipitation resistance' are more difficult to quantify since they are dependent on the poorly understood reaction mechanisms and precipitation kinetics in Li-S cells. While solvents with low Li_2S solubility could facilitate precipitation thereby potentially reducing both the electrolyte resistance and the 'precipitation resistance', the increased amount of insulating precipitates induce larger activation overpotentials. Large activation overpotentials could be mitigated through the use of nano-structured cathodes with high conductive surface area.

In the present work only a qualitative comparison between the model prediction and experimental data of cell discharge and electrolyte resistance curves can be made. This limitation is due to: (i) values for many physical parameters, especially those related to Li_2S precipitation and electrolyte conductivity, have not been obtained experimentally, nor are they established in the literature; (ii) the present model neglects the polysulfide shuttle as well as transport limitations that could occur at high currents, therefore it does not sufficiently capture the variation of discharge capacity with discharge current. However, improvements to existing modelling approaches have been presented which can qualitatively reproduce more features of a typical Li-S cell behavior than could be reproduced with previous models. These improvements are easy to add to any existing Li-S model to ensure better agreement with the observed cell performance.

4. Conclusion

In summary, we have demonstrated a lumped mechanistic model for Li-S cells considering electrochemical and precipitation reactions, activation overpotentials, electrolyte resistance, as well as morphology variations during discharge. The model is the first to the authors' knowledge to qualitatively reproduce the evolution of electrolyte resistance reported in the literature. The change in electrolyte resistance during discharge can be explained as the result of the concentration dependence of electrolyte conductivity in conjunction with ionic concentration variations due to precipitation. The increase in activation overpotential in the low plateau can be explained by the reduced electrochemical surface area, also associated with Li_2S precipitation. In addition, the limited rate of precipitation is shown to cause a drop in reduction potential, which manifests itself as a 'precipitation resistance'. In view of the central role that Li_2S precipitation plays in determining the operating voltage of Li-S batteries, future efforts should seek to develop an accurate understanding of precipitation mechanisms, as well as to measure the polysulfide solubility, precipitation rates, and the concentration-conductivity relation.

5. Acknowledgements

The authors would like to thank the Engineering and Physical Sciences Research Council in the UK for funding this work under the Revolutionary Electric Vehicle Battery (REVB) project EP/L505298/1.

6. Reference

[1] P. G. Bruce, S. A. Freunberger, L. J. Hardwick, J.-M. Tarascon, Li O 2 and Li S batteries with high energy storage, Nature Materials 11 (December) (2012) 19–30. doi:10.1038/NMAT3191.

[2] S. S. Zhang, Liquid electrolyte lithium/sulfur battery: Fundamental chemistry, problems, and solutions, Journal of Power Sources 231 (2013) 153–162. doi:10.1016/j.jpowsour.2012.12.102.
URL http://linkinghub.elsevier.com/retrieve/pii/S0378775312019568

[3] D. Bresser, S. Passerini, B. Scrosati, Recent progress and remaining challenges in sulfur-based lithium secondary batteries–a review., Chemical communications (Cambridge, England) 49 (90) (2013) 10545–62. doi:10.1039/c3cc46131a.
URL http://www.ncbi.nlm.nih.gov/pubmed/24100379

[4] V. S. Kolosnitsyn, E. V. Karaseva, Lithium-sulfur batteries: Problems and solutions, Russian Journal of Electrochemistry 44 (5) (2008) 506–509. doi:10.1134/S1023193508050029.
URL http://link.springer.com/10.1134/S1023193508050029

[5] X. Feng, M.-K. Song, W. C. Stolte, D. Gardenghi, D. Zhang, X. Sun, J. Zhu, E. J. Cairns, J. Guo, Understanding the degradation mechanism of rechargeable lithium/sulfur cells: a comprehensive study of the sulfur-graphene oxide cathode after discharge-charge cycling, Phys. Chem. Chem. Phys. 16 (2014) 16931–16940. doi:10.1039/C4CP01341G.
URL http://dx.doi.org/10.1039/C4CP01341G

[6] S. H. Thomke, Simulation, learning and R&D performance: Evidence from automotive development, Research Policy 27 (1998) 55–74. doi:10.1016/S0048-7333(98)00024-9.

[7] M. C. Becker, P. Salvatore, F. Zirpoli, The impact of virtual simulation tools on problem-solving and new product development organization, Research Policy 34 (2005) 1305–1321. doi:10.1016/j.respol.2005.03.016.

[8] Y. V. Mikhaylik, J. R. Akridge, Polysulfide Shuttle Study in the Li/S Battery System, Journal of The Electrochemical Society 151 (11) (2004) A1969. doi:10.1149/1.1806394.
URL http://jes.ecsdl.org/cgi/doi/10.1149/1.1806394

[9] K. Kumaresan, Y. Mikhaylik, R. E. White, A Mathematical Model for a LithiumSulfur Cell, Journal of The Electrochemical Society 155 (8) (2008) A576. doi:10.1149/1.2937304.
URL http://jes.ecsdl.org/cgi/doi/10.1149/1.2937304

[10] M. Ghaznavi, P. Chen, Sensitivity analysis of a mathematical model of lithiumsulfur cells part I: Applied discharge current and cathode conductivity, Journal of Power Sources 257 (2014) 394–401. doi:10.1016/j.jpowsour.2013.10.135.
URL http://linkinghub.elsevier.com/retrieve/pii/S0378775313018028

[11] M. Ghaznavi, P. Chen, Sensitivity analysis of a mathematical model of lithiumsulfur cells: Part II: Precipitation reaction kinetics and sulfur content, Journal of Power Sources 257 (2014) 402–411. doi:10.1016/j.jpowsour.2013.12.145.
URL http://linkinghub.elsevier.com/retrieve/pii/S0378775314001219

[12] M. Ghaznavi, P. Chen, Analysis of a Mathematical Model of Lithium-Sulfur Cells Part III: Electrochemical Reaction Kinetics, Transport Properties and Charging, Electrochimica Acta 137 (2014) 575–585. doi:10.1016/j.electacta.2014.06.033.
URL http://dx.doi.org/10.1016/j.electacta.2014.06.033

[13] D. N. Fronczek, W. G. Bessler, Insight into lithiumsulfur batteries: Elementary kinetic modeling and impedance simulation, Journal of Power Sources (2013) 6–11doi:10.1016/j.jpowsour.2013.02.018.
URL http://linkinghub.elsevier.com/retrieve/pii/S0378775313002814

[14] A. F. Hofmann, D. N. Fronczek, W. G. Bessler, Mechanistic modeling of polysulfide shuttle and capacity loss in lithium-sulfur batteries, Journal of Power Sourcesdoi:10.1016/j.jpowsour.2014.02.082.
URL http://linkinghub.elsevier.com/retrieve/pii/S0378775314002754

[15] V. S. Kolosnitsyn, E. V. Kuz'mina, E. V. Karaseva, S. E. Mochalov, Impedance spectroscopy studies of changes in the properties of lithium-sulfur cells in the course of cycling, Russian Journal of Electrochemistry 47 (7) (2011) 793–798. doi:10.1134/S1023193511070093.
URL http://link.springer.com/10.1134/S1023193511070093

[16] V. Kolosnitsyn, E. Kuzmina, E. Karaseva, S. Mochalov, A study of the electrochemical processes in lithiumsulphur cells by impedance spectroscopy, Journal of Power Sources 196 (3) (2011) 1478–1482. doi:10.1016/j.jpowsour.2010.08.105.
URL http://linkinghub.elsevier.com/retrieve/pii/S0378775310015909

[17] Z. Deng, Z. Zhang, Y. Lai, J. Liu, J. Li, Y. Liu, Electrochemical Impedance Spectroscopy Study of a Lithium/Sulfur Battery: Modeling and Analysis of Capacity Fading, Journal of the Electrochemical Society 160 (4) (2013) A553–A558. doi:10.1149/2.026304jes.
URL http://jes.ecsdl.org/cgi/doi/10.1149/2.026304jes

[18] N. A. Cañas, K. Hirose, B. Pascucci, N. Wagner, K. A. Friedrich, R. Hiesgen, Investigations of lithiumsulfur batteries using electrochemical impedance spectroscopy, Electrochimica Acta 97 (2013) 42–51. doi:10.1016/j.electacta.2013.02.101.
URL http://linkinghub.elsevier.com/retrieve/pii/S0013468613003460

[19] C. Barchasz, J.-C. Leprêtre, F. Alloin, S. Patoux, New insights into the limiting parameters of the Li/S rechargeable cell, Journal of Power Sources 199 (2012) 322–330. doi:10.1016/j.jpowsour.2011.07.021.
URL http://linkinghub.elsevier.com/retrieve/pii/S0378775311013590

[20] D. R. Chang, S. H. Lee, S. W. Kim, H. T. Kim, Binary electrolyte based on tetra(ethylene glycol) dimethyl ether and 1,3-dioxolane for lithium-sulfur battery, Journal of Power Sources 112 (2002) 452–460. doi:10.1016/S0378-7753(02)00418-4.

[21] H. Yamin, E. Peled, Electrochemistry of a nonaqueous lithium/sulfur cell, Journal of Power Sources 9 (1983) 281–287. doi:10.1016/0378-7753(83)87029-3.

[22] M. Park, X. Zhang, M. Chung, G. B. Less, A. M. Sastry, A review of conduction phenomena in Li-ion batteries, Journal of Power Sources 195 (2010) 7904–7929. doi:10.1016/j.jpowsour.2010.06.060.
URL http://dx.doi.org/10.1016/j.jpowsour.2010.06.060

[23] R. Xu, I. Belharouak, X. Zhang, R. Chamoun, C. Yu, Y. Ren, A. Nie, R. Shahbazian-Yassar, J. Lu, J. C. Li, K. Amine, Insight into sulfur reactions in lis batteries, ACS Applied Materials & Interfaces 6 (24) (2014) 21938–21945, pMID: 25425055. arXiv:http://dx.doi.org/10.1021/am504763p, doi:10.1021/am504763p.
URL http://dx.doi.org/10.1021/am504763p

[24] M. R. Busche, P. Adelhelm, H. Sommer, H. Schneider, K. Leitner, J. Janek, Systematical electrochemical study on the parasitic shuttle-effect in lithium- sulfur-cells at different temperatures and different rates, Journal of Power Sourcesdoi:10.1016/j.jpowsour.2014.02.075.
URL http://linkinghub.elsevier.com/retrieve/pii/S0378775314002687

[25] J. Brückner, S. Thieme, H. T. Grossmann, S. Dörfler, H. Althues, S. Kaskel, Lithiumsulfur batteries: Influence of c-rate, amount of electrolyte and

sulfur loading on cycle performance, Journal of Power Sources 268 (2014) 82 – 87. doi:http://dx.doi.org/10.1016/j.jpowsour.2014.05.143.
URL http://www.sciencedirect.com/science/article/pii/S0378775314008441

7. Figure captions

Fig. 1: (a) Electrolyte resistance (R_s) measured from a pouch Li-S cell manufactured by Oxis Energy Ltd. Galvanostatic EIS measurements were performed during a 0.34 A cell discharge, and the series resistance was extracted as the high-frequency x-axis intercept of the Nyquist plots at different depths of discharge. (b) Simulated R_s from the Kumaresan model [9] for a Li-S cell with similar energy capacity; model parameters are taken from Ghaznavi and Chen [12].

Fig. 2: (a) Electrolyte conductivity as a function of Li^+ concentration according to Eq. 16. (b) Simulated concentration of Li^+ during a 0.15C (0.34 A) discharge. (c) Simulated cell voltages and (d) simulated electrolyte resistances during discharge at 0.15 C and 0.03 C.

Fig. 3: Simulated activation overpotentials η_2 (for reaction Eq. 2) and η_6 (for Eq. 6) at 0.2C, and the specific electrochemical surface area (a_v) during discharge.

Fig. 4: The simulated reduction potential E_6 at 0.15C (solid line) and 0.03C (dashed line), and same potential calculated without considering Li_2S precipitation (symbols). ΔE_6 indicates the shift in E_6 caused by the difference in discharge current.

8. Tables and Figures

Table 1: Model parameters.

Kinetic & thermodynamic parameters	
$E_1^{\ominus}, E_2^{\ominus}, E_3^{\ominus}, E_4^{\ominus}, E_5^{\ominus}, E_6^{\ominus}$ (V)	$0.0,\ 2.38, 2.24, 2.15, 2.05, 1.94$
$i_2^0, i_3^0, i_4^0, i_5^0, i_6^0$ (Am^{-2})	$2.0, 1.5, 1.0, 0.6, 0.3$
k_p ($\mathrm{m}^6\ \mathrm{mol}^{-2}\ \mathrm{s}^{-1}$)	1.5×10^{-5}
K_{sp} ($\mathrm{mol}^3\ \mathrm{m}^{-9}$)	1.0×10^3
Initial conditions	
$C_{\mathrm{Li}^+,0}$, C_{S_8} ($\mathrm{mol\ m}^{-3}$)	$1.1 \times 10^3, 6.7 \times 10^2$
$C_{\mathrm{S}_8^{2-}}, C_{\mathrm{S}_6^{2-}}, C_{\mathrm{S}_4^{2-}}, C_{\mathrm{S}_2^{2-}}, C_{\mathrm{S}^{2-}}$ ($\mathrm{mol\ m}^{-3}$)	$1.0 \times 10^2, 8.2, 5.6 \times 10^{-3}, 8.0 \times 10^{-6}, 1.4 \times 10^{-8}$
$v_{\mathrm{Li_2S}}$	10^{-7}
ε_0	0.65
σ_0 ($\mathrm{S\ m}^{-1}$)	2.0×10^{-3}
Geometric & other parameters	
A (m^2)	0.29
a_v^0 (m^{-1})	1.0×10^5
b ($\mathrm{S\ m}^2\ \mathrm{mol}^{-1}$)	4.6×10^{-7}
l (m)	2×10^{-5}
$V_{\mathrm{Li_2S}}$ ($\mathrm{m}^3\ \mathrm{mol}^{-1}$)	2.8×10^{-6}
ξ	6

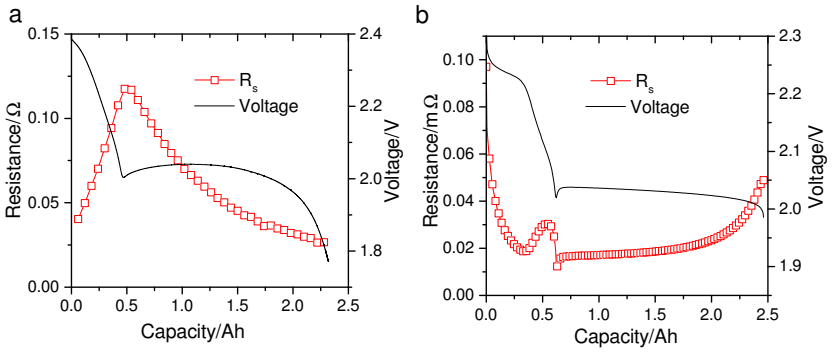

Figure 1: (a) Electrolyte resistance (R_s) measured from a pouch Li-S cell manufactured by Oxis Energy Ltd. Galvanostatic EIS measurements were performed during a 0.34 A cell discharge, and the series resistance was extracted as the high-frequency x-axis intercept of the Nyquist plots at different depths of discharge. (b) Simulated R_s from the Kumaresan model [9] for a Li-S cell with similar energy capacity; model parameters were taken from Ghaznavi and Chen [12].

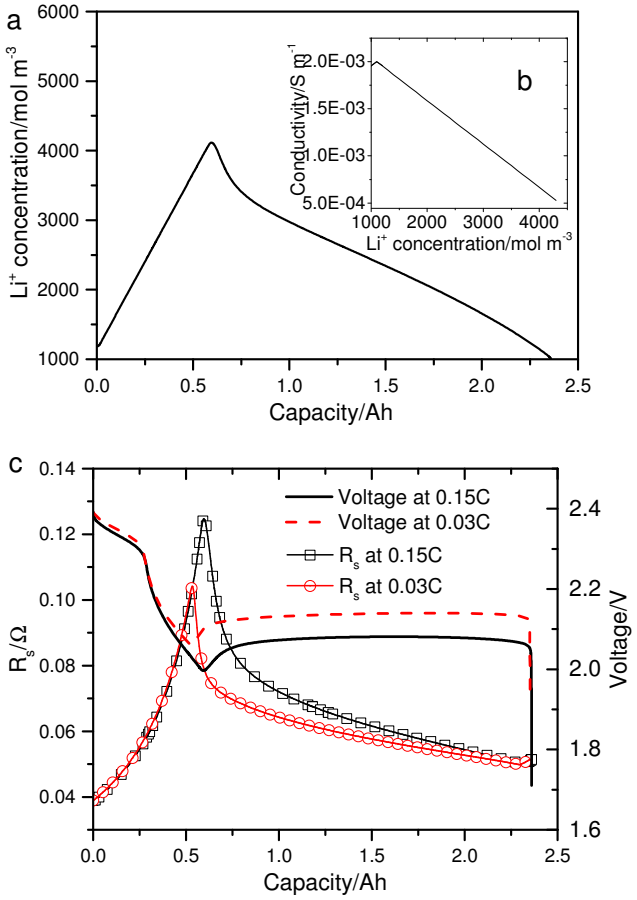

Figure 2: (a) Simulated concentration of Li^+ during 0.15C discharge. Inset (b) shows the electrolyte conductivity as a function of Li^+ concentration according to Eq. 16. (c) Simulated discharge voltages (symbols) and electrolyte resistances (lines) at 0.15 C and 0.03 C.

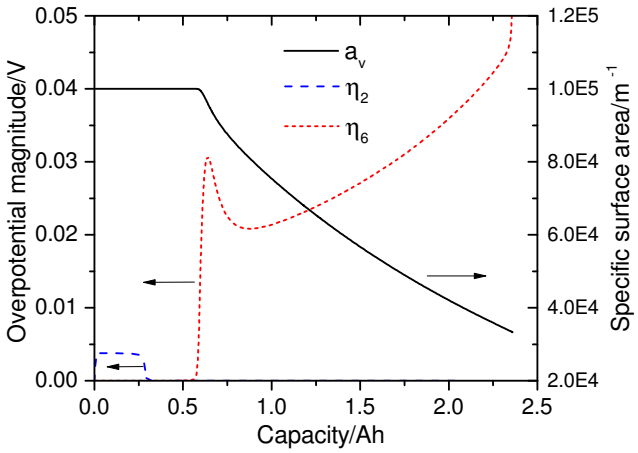

Figure 3: Simulated activation overpotentials η_2 (for reaction Eq. 2) and η_6 (for Eq. 6) during 0.15C discharge, and the specific electrochemical surface area (a_v) during discharge.

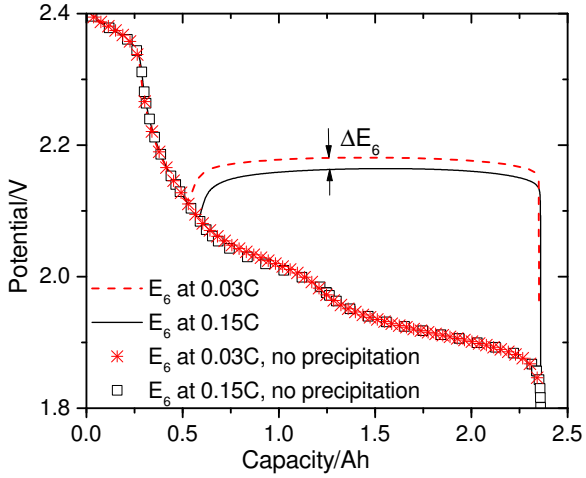

Figure 4: The simulated reduction potential E_6 during 0.15C (solid line) and 0.03C (dashed line) discharge, and same potential calculated without considering Li_2S precipitation (symbols). ΔE_6 indicates the shift in reduction potential caused by the difference in discharge current.